

Very large thermal rectification in ferromagnetic insulator-based superconducting tunnel junctions

F. Giazotto^{1, a)} and F. S. Bergeret^{2, 3, b)}

¹⁾NEST Istituto Nanoscienze-CNR and Scuola Normale Superiore, I-56127 Pisa, Italy

²⁾Centro de Fisica de Materiales (CFM-MPC), Centro Mixto CSIC-UPV/EHU, Manuel de Lardizabal 5, 20018 Donostia-San Sebastian, Spain

³⁾Donostia International Physics Center (DIPC), Manuel de Lardizabal, 4, 20018, Donostia San Sebastian, Spain

We investigate electronic thermal rectification in ferromagnetic insulator-based superconducting tunnel junctions. Ferromagnetic insulators coupled to superconductors are known to induce sizable spin splitting in the superconducting density of states, and also lead to efficient spin filtering if operated as tunnel barriers. The combination of spin splitting and spin filtering is shown to yield a substantial *self-amplification* of the electronic heat diode effect due to breaking of the electron-hole symmetry in the system which is added to the thermal asymmetry of the junction. Large spin splitting and large spin polarization can potentially lead to thermal rectification efficiency exceeding $\sim 5 \times 10^4\%$ for realistic parameters in a suitable temperature range, thereby outperforming up to a factor of ~ 250 the heat diode effect achievable with conventional superconducting tunnel junctions. These results could be relevant for improved mastering of the heat currents in innovative phase-coherent caloritronic nanodevices, and for enhanced thermal management of quantum circuits at the nanoscale.

A *thermal* rectifier, or heat diode,^{1,2} is a device in which the heat current depends on the sign and the amplitude of the temperature gradient imposed across it. The implementation of efficient heat diodes would represent a breakthrough in the realization of improved thermal circuits for cooling³, thermal isolation, energy harvesting, radiation sensing, and several other applications⁴. Recently, the control of thermal transport at the nanoscale has been attracting great interest³⁻⁶. From the theoretical side, strong effort has been put to conceive thermal rectification setups dealing with phonons⁷⁻¹⁰, electrons^{6, 11-20} and photons²¹. Experimentally, promising results were obtained so far in the context of electronic²²⁻²⁴ and phononic²⁵⁻²⁷ heat transport. Rectification of electronic heat currents has been studied in several types of tunneling junctions between different materials such as, for instance, normal metals¹⁷, Josephson junctions¹⁸, and superconductor-normal metal structures^{6, 19}. In all cases, heat rectification stems from thermal asymmetry of the structure in the direction of the current flow. In conventional superconducting tunnel junctions this asymmetry together with the highly non-linear temperature dependence of the density of states leads to a heat rectification up to $\sim 800\%$ in Josephson junctions¹⁸.

In this letter we study thermal rectification effects in systems based on ferromagnetic insulator (FI) superconducting tunnel junctions. The combination of spin splitting and spin polarization induced by FIs breaks the electron-hole symmetry of the electronic transport. This electron-hole symmetry breaking (EHSB) together with non-linear temperature dependence of the superconducting spectral properties leads to an unrivalled heat diode effect with a suitable choice of realistic parameters. Specifically, a rectification efficiency exceeding $\sim 5 \times 10^4\%$ can be obtained, outperforming up to a factor of ~ 250 that achievable in conventional superconducting tunnel

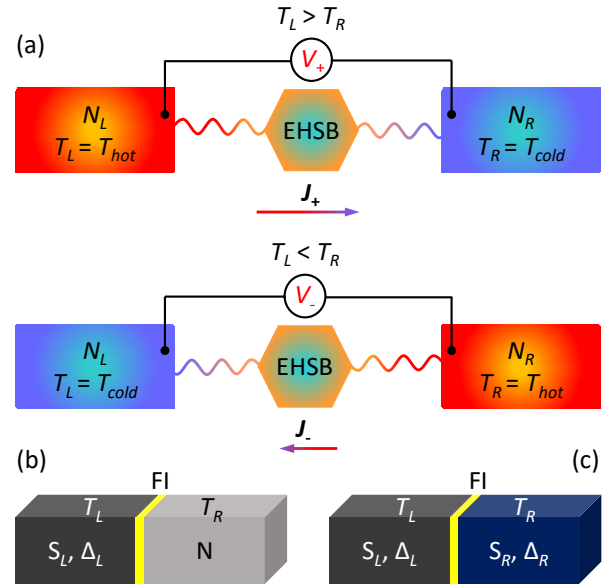


FIG. 1. (a) Sketch of two electronic reservoirs (either normal or superconducting) with different temperature-dependent density of states $N_{L,R}$ residing at temperature $T_{L,R}$. The reservoirs are coupled to an element that breaks electron-hole symmetry. This leads to a thermoelectric response, and enhanced *thermal* rectification. J_+ and J_- represent the heat flow in the forward ($T_L > T_R$) and reverse ($T_L < T_R$) thermal-bias configuration, respectively, while V_+ and V_- denote the corresponding thermovoltages developed across the system. (b) Prototypical ferromagnetic insulator (FI)-based superconductor (S_L)-normal metal (N) and (c) superconductor (S_L)-superconductor (S_R) tunnel junctions. The FI is inserted in the structures as a tunnel barrier so to induce both a spin splitting in the density of states of the superconductor, and to provide a spin filtering effect. Δ_L (Δ_R) denotes the energy gap in S_L (S_R).

junctions. These results could be relevant for improved thermal isolation of cryogenic quantum circuitry at the nanoscale.

Setup and basic equations Figure 1(a) schematizes the

^{a)}Electronic mail: francesco.giazotto@sns.it

^{b)}Electronic mail: fs.bergeret@csic.es

generic system under investigation which consists of two electronic reservoirs (either superconducting or normal metallic) residing at temperature $T_{L,R}$. The density of states $N_{L,R}$ depends on the temperature and applied exchange field. The two electrodes are electrically coupled via an EHSB mechanism. The latter gives rise to a thermoelectric response in the system, and to a thermovoltage amplitude V_+ (V_-) developed for $T_L > T_R$ ($T_L < T_R$). The heat current flowing in the forward thermal-bias configuration is denoted with J_+ whereas J_- denotes the one flowing in the reverse thermal-bias configuration. As we shall show, the presence of EHSB in the system yields a *self-amplification* of thermal rectification efficiency up to unparalleled values for suitable parameters of the structure, and proper thermal bias conditions. The EHSB mechanism can be achieved by placing a S_L FIN, [Fig. 1(b)] and a S_L FIS $_R$, [Fig. 1(c)] tunnel junctions. The presence of the FI layer yields both spin splitting of the density of states in S_L and spin filtering at the barrier. The combination results in the EHSB mechanism^{28–34}.

The interaction between the spin of conducting electrons in the superconductor and the localized magnetic moments in the adjacent FI leads to an effective exchange interaction (h_{exc}) in the superconductor. This field decays away from the S/FI interface over the superconducting coherence length ξ_0 ³⁵. Yet, we assume that the superconducting layer thickness is smaller than ξ_0 , so that the induced h_{exc} in the superconductor by FI is spatially homogeneous. In this situation, the spin-dependent normalized density of states of the superconductor is simply given by $N^{\uparrow,\downarrow}(E) = \frac{1}{2}|\text{Re}[\frac{E+i\Gamma\pm h_{exc}}{\sqrt{(E+i\Gamma\pm h_{exc})^2-\Delta^2}}]|$, where Γ is the Dynes parameter, and Δ is the superconducting gap which depends on T and h_{exc} via the self-consistency equation $\ln(\frac{\Delta_0}{\Delta}) = \int_0^{\hbar\omega_D} dE \frac{f_+(E)+f_-(E)}{\sqrt{E^2+\Delta^2}}$, where $f_{\pm}(E) = \{1 + \exp[\frac{1}{k_B T}(\sqrt{E^2+\Delta^2} \mp h_{exc})]\}^{-1}$, ω_D is the Debye frequency of the superconductor, $\Delta_0 = 1.764k_B T_c$ is the zero-temperature, zero-exchange field superconducting pairing potential, T_c is the critical temperature, and k_B is the Boltzmann constant. The parameter Γ accounts for the broadening of the coherent peaks in the density of states due to inelastic scattering, and for an ideal superconductor $\Gamma \rightarrow 0$ ³⁶. In all the calculations we set $\Gamma = 10^{-4}\Delta_0$, unless differently stated.

We are interested in both the DC charge and electronic heat currents through the junctions which are given by³⁰ $I = \frac{1}{eR_T} \int_{-\infty}^{\infty} dE [N_+ + PN_-] [f_L(V, T_L) - f_R(T_R)]$, and $J = \frac{1}{eR_T} \int_{-\infty}^{\infty} dE (E + eV) [N_+ + PN_-] [f_L(V, T_L) - f_R(T_R)]$, respectively. Here, R_t is the normal-state tunneling resistance of the junction, $N_{\pm} = (N_L^{\uparrow} N_R^{\uparrow} \pm N_L^{\downarrow} N_R^{\downarrow})$, and $0 \leq P \leq 1$ is the barrier spin polarization provided by the FI layer³⁷. Moreover, $f_L(V, T_L) = [1 + \exp[(E + eV)/k_B T_L]]^{-1}$ and $f_R(T_R) = [1 + \exp(E/k_B T_R)]^{-1}$ are the equilibrium quasi-particle distribution functions, and e is the electron charge. In principle the expressions for both currents may contain a phase-dependent term^{4,5,38}. However, since our system exhibits a thermovoltage across the junction the phase becomes time-dependent and thereby not contributing to DC transport.

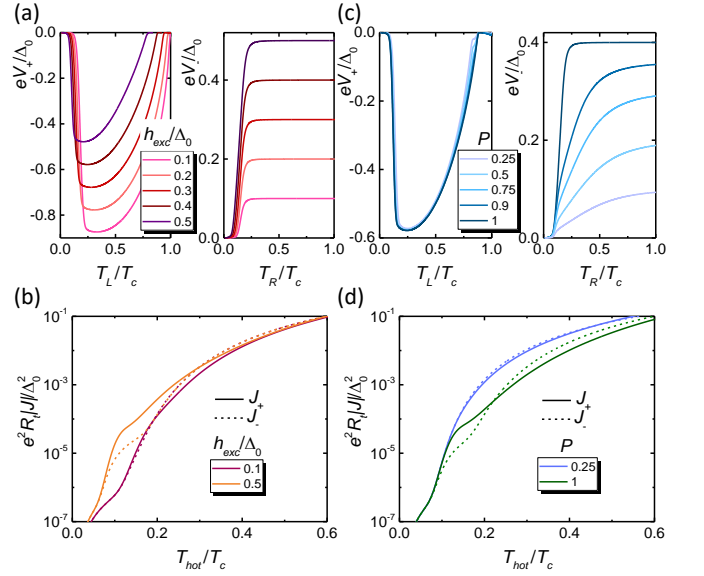


FIG. 2. (a) Thermovoltage V_+ vs T_L (left panel) and V_- vs T_R (right panel) calculated for a S_L FIN junction at $P = 1$ and $T_R = 0.01T_c$ (left panel) and $T_L = 0.01T_c$ (right panel) for different values of the exchange field h_{exc} . (b) Absolute value of the heat current $|J|$ vs T_{hot} flowing through a S_L FIN junction calculated at $P = 1$ and $T_{cold} = 0.01T_c$ for two selected values of h_{exc} . (c) V_+ vs T_L (left panel) and V_- vs T_R (right panel) calculated for a S_L FIN junction at $h_{exc} = 0.4\Delta_0$ and $T_R = 0.01T_c$ (left panel) and $T_L = 0.01T_c$ (right panel) for different values of barrier polarization P . (d) Absolute value of the heat current $|J|$ vs T_{hot} flowing through a S_L FIN junction calculated at $h_{exc} = 0.4\Delta_0$ and $T_{cold} = 0.01T_c$ for two selected values of P .

It is also worth emphasizing that the values of both spin polarization and spin splitting can be extracted from experiments, as demonstrated in several works^{39–48}.

We assume that both electronic reservoirs are thermalized with well defined temperatures $T_{L,R}$. In the *forward* thermal bias configuration [see Fig. 1(a)], a thermal gradient is intentionally created at the junction by setting $T_L = T_{hot} > T_R = T_{cold}$, which leads to a total heat flux J_+ through the system. In the *reverse* thermal bias configuration, the heat gradient is inverted so that $T_L = T_{cold} < T_R = T_{hot}$ yielding a total heat current J_- flowing from the right to the left electrode. The electronic thermal rectification efficiency is defined as $R(\%) = 100 \times (|J_+| - |J_-|)/|J_-|$, such that the absence of heat rectification corresponds to $R = 0$ and $R > 0$ indicates a preferential heat flow from the left to the right side of the junction. In order to determine the thermal rectification, for example in the forward thermal bias configuration, for arbitrary $T_L > T_R$ we need first to determine the thermovoltage V_+ across the junction by solving the equation $I(V_+, T_L, T_R) = 0$. Then, the obtained thermovoltage is used to compute the corresponding heat current $J_+(V_+, T_L, T_R)$ flowing through the junction. In the reverse thermal bias condition, $T_R > T_L$, the same procedure is performed to determine V_- and J_- . Following this procedure we determine R in both junction setups depicted in Figs. 1(b-c).

*S_L*FIN tunnel junction It is instructive to start our discus-

sion by analyzing the setup of Fig. 1(b), the S_L FIN superconducting tunnel junction. A thermal bias across the structure leads to a thermovoltage V_{\pm} which depends on the sign of the thermal gradient itself, and stems from EHSB in the junction⁴⁹ [see Fig. 1(a)]. In particular, the thermovoltage V_+ vs T_L (at $T_R = 0.01T_c$) is shown in the left panel of Fig. 2(a) whereas V_- vs T_R (at $T_L = 0.01T_c$) is shown in the right panel of the same figure, both evaluated at $P = 1$ for selected values of the exchange field h_{exc} . Beside the substantial difference between the thermovoltage amplitudes V_+ and V_- for the same exchange field, V_+ is a non-monotonic function of T_L , vanishing when the superconducting pairing potential goes to zero, while V_- monotonically increases with T_R , saturating at the asymptotic value $eV_- = h_{exc}$ at large temperature⁴⁹. This sizable difference between the thermovoltages has a direct impact on the corresponding heat currents J_{\pm} flowing through the junction. These are shown in Fig. 2(b) for two given values of the exchange field. For the larger value of h_{exc} the difference between the forward and reverse heat currents is increased thereby leading to enhanced thermal rectification in the S_L FIN junction. This difference appears to be particularly pronounced for $0.1T_c \lesssim T_{hot} \lesssim 0.2T_c$, which is indeed the temperature range where the maximum thermovoltage amplitudes develop across the junction [cf. Fig. 2(a)].

Left panel of Fig. 2(c) displays V_+ vs T_L (at $T_R = 0.01T_c$) while the right one shows V_- vs T_R (at $T_L = 0.01T_c$) both calculated at $h_{exc} = 0.4\Delta_0$ for a different values of P . The thermovoltage V_+ is negligibly affected by the polarization showing a shape very similar to that obtained for the same value of h_{exc} in panel (a). By contrast, V_- is strongly affected by P , and becomes larger by increasing the barrier polarization. Also in the present case of finite barrier polarization the large difference of thermovoltage amplitudes deeply affect the corresponding heat currents flowing through the structure, as shown in Fig. 2(d) for two selected values of P . A large barrier polarization ($P \sim 1$) strongly enhances the difference between forward and reverse heat currents, therefore leading to a sizable heat diode effect in the junction.

In Figure 3 we show the rectification efficiency for the S_L FIN junction. Specifically, 3(a) shows the heat rectification efficiency R vs T_{hot} calculated for zero barrier polarization at $T_{cold} = 0.01T_c$ for different values of h_{exc} . The absence of spin polarization at the barrier leads to a zero thermoelectric voltage. The increase of h_{exc} yields a slight reduction of R compared to that of a conventional SIN tunnel junction (i.e., for $h_{exc} = 0$)^{6,18,19}, allowing to obtain a maximum rectification efficiency of $\sim 22\%$ for $h_{exc} = 0.5\Delta_0$ at $T_{hot} \sim 0.5T_c$. The above heat rectification reduction stems from a larger contribution to the heat transport for electrons with energy close to the Fermi level at large h_{exc} . This contribution restore the thermal symmetry of the junction, and hence reduces the heat rectification. In addition, there are additional features appearing in the rectification characteristics at higher temperatures which occur when superconductivity is quenched due to the presence of a finite exchange field. In short, Fig. 3(a) demonstrates that spin-splitting alone cannot improve thermal rectification with respect to conventional superconducting junctions.

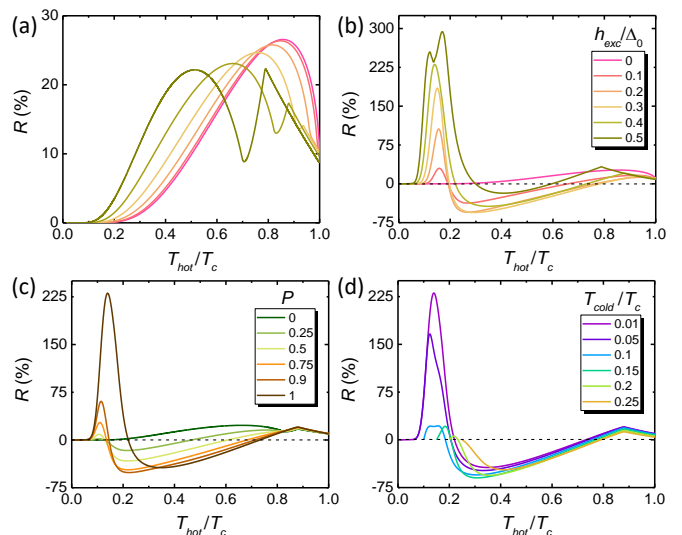


FIG. 3. Thermal rectification coefficient R for the S_L FIN junction. (a) Thermal rectification coefficient R vs T_{hot} calculated at $T_{cold} = 0.01T_c$ and $P = 0$ for different values of the exchange field h_{exc} . (b) The same as in panel (a) but for barrier polarization $P = 1$. (c) R vs T_{hot} calculated at $T_{cold} = 0.01T_c$ and $h_{exc} = 0.4\Delta_0$ for several values of P . (d) R vs T_{hot} calculated at $h_{exc} = 0.4\Delta_0$ and $P = 1$ for several values of T_{cold} . Dashed lines indicate $R = 0$.

However, if the barrier spin-polarization is finite the situation changes drastically. The role of finite h_{exc} at $P = 1$ is shown in Fig. 3(b). In particular, the thermoelectric response of the junction is increased in the presence of high exchange field allowing to obtain both large heat rectification in the forward thermal-bias configuration for $h_{exc} = 0.5\Delta_0$ (i.e., up to $\sim 290\%$) and a sizable contribution in the reverse thermal-bias configuration (around $\sim -55\%$ for $h_{exc} = 0.3\Delta_0$). All the above results prove that the presence of an EHSB mechanisms in the S_L FIN junction leads to a substantial *self-amplification* of the heat diode efficiency which now obtains values which are larger by more than a factor of ~ 10 than those typically achievable in conventional superconducting tunnel junctions^{6,18,19}.

The impact of a finite barrier polarization at $h_{exc} = 0.4\Delta_0$ is displayed in Fig. 3(c) for different values of P . The effect is similar to that caused by an increasing exchange field [see Fig. 3(c)], and shows the relevance of a large spin polarization in order to achieve a sizable heat rectification. For instance, R turns out to be suppressed by more than a factor of ~ 20 if P is reduced down to 50%. Finally, the effect of the smaller temperature T_{cold} onto R is displayed in Fig. 3(d) as a function of T_{hot} . We notice, in particular, the strong suppression of R occurring by increasing T_{cold} : for instance, R is suppressed by roughly one order of magnitude at $T_{cold} = 0.1T_c$. This emphasizes the requirement of a sufficiently low T_{cold} in order to achieve large rectification effects.

S_L FIS_R tunnel junction We now discuss the heat diode effect in the junction setup sketched in Fig. 1(c). For simplicity we assume the two superconductors are identical such that they have the same zero-temperature, zero-exchange field en-

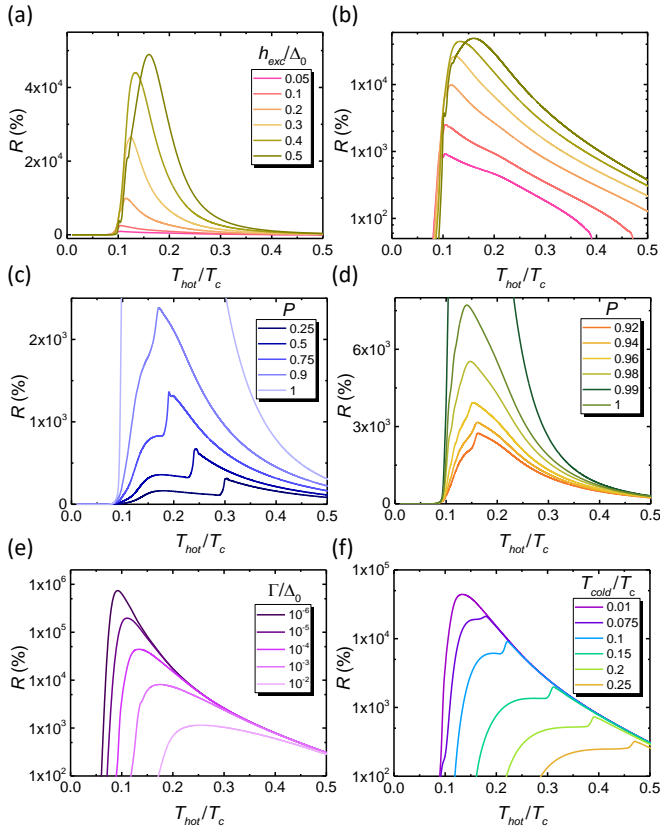


FIG. 4. Thermal rectification coefficient R for the S_LFIS_R junction. (a) R vs T_{hot} calculated at $T_{cold} = 0.01T_c$ and $P = 1$ for different values of the exchange field h_{exc} . (b) The same as in panel (a) but shown on a logarithmic scale. (c) R vs T_{hot} calculated at $T_{cold} = 0.01T_c$ and $h_{exc} = 0.4\Delta_0$ for a few values of P . (d) R vs T_{hot} calculated at $T_{cold} = 0.01T_c$ and $h_{exc} = 0.4\Delta_0$ for several high values of barrier polarization in the range $0.92 \leq P \leq 1$. (e) R vs T_{hot} calculated at $T_{cold} = 0.01T_c$, $h_{exc} = 0.4\Delta_0$, and $P = 1$ for a few values of Γ . (f) R vs T_{hot} calculated at $h_{exc} = 0.4\Delta_0$ and $P = 1$ for different values of T_{cold} .

ergy gap Δ_0 . To maximize the thermal asymmetry, we also assume that only the density of states of the left electrode (N_L) is affected by h_{exc} so to break the thermal symmetry of the system. Such an asymmetry can be achieved by inserting a very thin non-magnetic oxide layer at the FI/S_R interface⁴⁰. This implies that $N_R^\uparrow = N_R^\downarrow$. We now define the rectification efficiency as $R = 100 \times (|J_-| - |J_+|)/|J_+|$ so to easily compare the two different junction setups since, as we shall show, J_- is typically much larger than J_+ in the S_LFIS_R junction. Figures 4(a) and (b) show the impact of a finite h_{exc} on R at $P = 1$. In particular, we note the very large thermal rectification which can be obtained, up to $\sim 5 \times 10^4\%$ for $h_{exc} = 0.5\Delta_0$ at $T_{hot} \simeq 0.15T_c$. This value is ~ 250 times larger than the one achievable in conventional all-superconducting tunnel junctions made with superconductors with different energy gaps^{6,18}. Yet, even for moderate h_{exc} values (i.e., $h_{exc} = 0.2\Delta_0$) R can reach values as large as $10^4\%$ in the suitable T_{hot} range. The above results demonstrate the effectiveness of S_LFIS_R tunnel junctions to achieve

very high thermal rectification efficiency.

The role of P is displayed in Figs. 4(c) and (d), and reveal the increased robustness of the S_LFIS_R setup with respect to the S_LFIN one in terms of limited barrier polarization. For example, for a moderate spin polarization, $P = 75\%$, we still get a sizable $R \simeq 1370\%$ which is about two times larger than the maximum value achievable in conventional SIS tunnel junctions^{6,18}. Nowadays, for instance, state-of-the-art ferromagnetic europium (Eu) chalcogenides tunnel barriers can provide spin polarization close to 100%⁵⁰ which would make thermal rectification efficiencies larger than $\sim 7.5 \times 10^3\%$ readily available in superconducting tunnel junction setups operating at cryogenic temperatures.

The impact of non-idealities of the junction is shown in Fig. 4(e) where R is plotted against T_{hot} for a few selected values of Γ . From a quantitative point of view, thermal rectification efficiency turns out to be less effective the larger the value of Γ . In particular, for a sizable $\Gamma = 10^{-2}\Delta_0$, the maximum of R is reduced down to $\sim 1140\%$ at $T_{hot} \simeq 0.25T_c$. This fact emphasizes the requirement of high-quality tunnel junctions in order to preserve a substantial heat diode effect. Finally, Fig. 4(f) shows how T_{cold} affects the rectification efficiency. Analogously to the S_LFIN setup, by increasing T_{cold} deeply suppresses the R coefficient, although in a reduced way. In particular, for $T_{cold} = 0.1T_c$ the rectification efficiency turns out to be decreased by almost a factor of 5 with respect to the lowest temperature, suggesting that the S_LFIS_R junction is more efficient as a heat diode at higher temperatures than the S_LFIN setup.

In summary, we have demonstrated theoretically the occurrence of unparalleled thermal diode effect in superconducting tunnel junctions with ferromagnetic insulators. In particular, thermal rectification efficiency above $\sim 5 \times 10^4\%$ could be achieved for realistic material parameters in a suitable temperature range. Such a heat rectifier efficiency exceeds by a factor of ~ 250 the one obtained with conventional superconducting tunnel junctions. Ideal materials for the heat rectifier are europium chalcogenides layers (EuO and EuS), for which values of P ranging from 80% up to $\sim 100\%$ have been reported^{37,40,42,51-55}, in combination with Al superconducting thin films⁴⁶⁻⁴⁸. Yet, very large spin-filtering has been reported in GdN barriers as well,⁵⁶⁻⁵⁸ with polarizations as large as 97% at low temperature. Our finding might be relevant for enhanced control of heat current in phase-coherent caloritronic devices^{4,5} as well as for general thermal management of nanoscale quantum circuits³.

The authors acknowledge the European Unions Horizon 2020 research and innovation programme under the grant agreement No. 800923-SUPERTEd and the Spanish Ministerio de Ciencia e Innovacion (MICINN) through the Project FIS2017-82804-P, for partial financial support.

¹N. A. Roberts and D. Walker, Int. J. Therm. Sci. **50**, 648 (2011).

²B. Li, L. Wang, and G. Casati, Phys. Rev. Lett. **93**, 184301 (2004).

³F. Giazotto, T. T. Heikkilä, A. Luukanen, A. M. Savin, and J. P. Pekola, Rev. Mod. Phys. **78**, 217 (2006).

⁴A. Fornieri and F. Giazotto, Nat. Nanotechnol. **12**, 944 (2017).

⁵M. Martínez-Pérez, P. Solinas, and F. Giazotto, J. Low Temp. Phys. **175**, 813 (2014).

- ⁶A. Fornieri, M. J. Martínez-Pérez, and F. Giazotto, *AIP Adv.* **5**, 053301 (2015).
- ⁷L.-A. Wu and D. Segal, *Phys. Rev. Lett.* **102**, 095503 (2009).
- ⁸D. Segal, *Phys. Rev. Lett.* **100**, 105901 (2008).
- ⁹B. Li, L. Wang, and G. Casati, *Appl. Phys. Lett.* **88**, 143501 (2006).
- ¹⁰M. Terraneo, M. Peyrard, and G. Casati, *Phys. Rev. Lett.* **88**, 094302 (2002).
- ¹¹R. López and D. Sánchez, *Phys. Rev. B* **88**, 045129 (2013).
- ¹²J. Ren and J.-X. Zhu, *Phys. Rev. B* **87**, 165121 (2013).
- ¹³L. Bours, B. Sothmann, M. Carrega, E. Strambini, A. Braggio, E. M. Hankiewicz, L. W. Molenkamp, and F. Giazotto, *Phys. Rev. Appl.* **11**, 044073 (2019).
- ¹⁴T. Ruokola and T. Ojanen, *Phys. Rev. B* **83**, 241404 (2011).
- ¹⁵T. Ruokola, T. Ojanen, and A.-P. Jauho, *Phys. Rev. B* **79**, 144306 (2009).
- ¹⁶D. M.-T. Kuo and Y.-c. Chang, *Phys. Rev. B* **81**, 205321 (2010).
- ¹⁷A. Fornieri, M. J. Martínez-Pérez, and F. Giazotto, *Appl. Phys. Lett.* **104**, 183108 (2014).
- ¹⁸M. Martínez-Pérez and F. Giazotto, *Appl. Phys. Lett.* **102**, 182602 (2013).
- ¹⁹F. Giazotto and F. Bergeret, *Appl. Phys. Lett.* **103**, 242602 (2013).
- ²⁰D. Goury and R. Sánchez, *Appl. Phys. Lett.* **115**, 092601 (2019).
- ²¹P. Ben-Abdallah and S.-A. Biehs, *Appl. Phys. Lett.* **103**, 191907 (2013).
- ²²M. J. Martínez-Pérez, A. Fornieri, and F. Giazotto, *Nat. Nanotechnol.* **10**, 303 (2015).
- ²³J. Senior, A. Gubaydullin, B. Karimi, J. T. Peltonen, J. Ankerhold, and J. P. Pekola, *Comm. Phys.* **3**, 1 (2020).
- ²⁴R. Scheibner, "M. k+ onig, d. reuter, ad wieck, c. gould, h. buhmann, lw molenkamp," *New J. Phys* **10**, 083016 (2008).
- ²⁵C. W. Chang, D. Okawa, A. Majumdar, and A. Zettl, *Science* **314**, 1121 (2006).
- ²⁶W. Kobayashi, Y. Teraoka, and I. Terasaki, *Appl. Phys. Lett.* **95**, 171905 (2009).
- ²⁷H. Tian, D. Xie, Y. Yang, T.-L. Ren, G. Zhang, Y.-F. Wang, C.-J. Zhou, P.-G. Peng, L.-G. Wang, and L.-T. Liu, *Sci. Rep.* **2**, 1 (2012).
- ²⁸F. S. Bergeret, M. Silaev, P. Virtanen, and T. T. Heikkilä, *Rev. Mod. Phys.* **90**, 041001 (2018).
- ²⁹T. T. Heikkilä, M. Silaev, P. Virtanen, and F. S. Bergeret, *Prog. Surf. Sci.* **94**, 100540 (2019).
- ³⁰A. Ozaeta, P. Virtanen, F. Bergeret, and T. Heikkilä, *Phys. Rev. Lett.* **112**, 057001 (2014).
- ³¹P. Machon, M. Eschrig, and W. Belzig, *Phys. Rev. Lett.* **110**, 047002 (2013).
- ³²P. Machon, M. Eschrig, and W. Belzig, *New J. Phys.* **16**, 073002 (2014).
- ³³S. Kolenda, M. J. Wolf, and D. Beckmann, *Phys. Rev. Lett.* **116**, 097001 (2016).
- ³⁴J. Linder and J. W. Robinson, *Nat. Phys.* **11**, 307 (2015).
- ³⁵T. Tokuyasu, J. A. Sauls, and D. Rainer, *Phys. Rev. B* **38**, 8823 (1988).
- ³⁶R. Dynes, J. Garno, G. Hertel, and T. Orlando, *Phys. Rev. Lett.* **53**, 2437 (1984).
- ³⁷J. S. Moodera, T. S. Santos, and T. Nagahama, *J. Phys.: Condens. Matter* **19**, 165202 (2007).
- ³⁸F. Giazotto and M. J. Martínez-Pérez, *Nature* **492**, 401 (2012).
- ³⁹R. Meservey and P. Tedrow, *Phys. Rep.* **238**, 173 (1994).
- ⁴⁰X. Hao, J. Moodera, and R. Meservey, *Phys. Rev. B* **42**, 8235 (1990).
- ⁴¹B. Li, G.-X. Miao, and J. S. Moodera, *Phys. Rev. B* **88**, 161105 (2013).
- ⁴²B. Li, N. Roschewsky, B. A. Assaf, M. Eich, M. Epstein-Martin, D. Heiman, M. Münzenberg, and J. S. Moodera, *Phys. Rev. Lett.* **110**, 097001 (2013).
- ⁴³Y. Xiong, S. Stadler, P. Adams, and G. Catelani, *Phys. Rev. Lett.* **106**, 247001 (2011).
- ⁴⁴T. Liu, J. Prestigiacomo, and P. Adams, *Phys. Rev. Lett.* **111**, 027207 (2013).
- ⁴⁵M. Wolf, C. Stürgers, G. Fischer, and D. Beckmann, *Phys. Rev. B* **90**, 144509 (2014).
- ⁴⁶E. Strambini, V. Golovach, G. De Simoni, J. Moodera, F. Bergeret, and F. Giazotto, *Phys. Rev. Mater.* **1**, 054402 (2017).
- ⁴⁷G. De Simoni, E. Strambini, J. S. Moodera, F. S. Bergeret, and F. Giazotto, *Nano Lett.* **18**, 6369 (2018).
- ⁴⁸M. Rouco, S. Chakraborty, F. Aikebaier, V. N. Golovach, E. Strambini, J. S. Moodera, F. Giazotto, T. T. Heikkilä, and F. S. Bergeret, *Phys. Rev. B* **100**, 184501 (2019).
- ⁴⁹F. Giazotto, P. Solinas, A. Braggio, and F. S. Bergeret, *Phys. Rev. Appl.* **4**, 044016 (2015).
- ⁵⁰J. S. Moodera, G.-X. Miao, and T. S. Santos, *Phys. Today* **63**, 46 (2010).
- ⁵¹J. Moodera, X. Hao, G. Gibson, and R. Meservey, *Phys. Rev. Lett.* **61**, 637 (1988).
- ⁵²T. S. Santos and J. S. Moodera, *Phys. Rev. B* **69**, 241203 (2004).
- ⁵³J. Moodera, R. Meservey, and X. Hao, *Phys. Rev. Lett.* **70**, 853 (1993).
- ⁵⁴T. Santos, J. Moodera, K. Raman, E. Negusse, J. Holroyd, J. Dvorak, M. Liberati, Y. Idzerda, and E. Arenholz, *Phys. Rev. Lett.* **101**, 147201 (2008).
- ⁵⁵G.-X. Miao and J. S. Moodera, *Appl. Phys. Lett.* **94**, 182504 (2009).
- ⁵⁶K. Senapati, M. G. Blamire, and Z. H. Barber, *Nat. Mater.* **10**, 849 (2011).
- ⁵⁷A. Pal, K. Senapati, Z. Barber, and M. Blamire, *Adv. Mater.* **25**, 5581 (2013).
- ⁵⁸A. Pal, Z. Barber, J. Robinson, and M. Blamire, *Nat. Commun.* **5**, 1 (2014).